# Ataluren Prevented Bone Loss Induced by Ovariectomy and Aging in Mice Through the BMP-SMAD Signaling Pathway

**Lijun Zeng**
Peking University School and Hospital of Stomatology: Peking University Hospital of Stomatology
**Ranli Gu**
Peking University School and Hospital of Stomatology: Peking University Hospital of Stomatology
**Yuzi Shao**
Peking University School and Hospital of Stomatology: Peking University Hospital of Stomatology
**Yuan Zhu**
Peking University School and Hospital of Stomatology: Peking University Hospital of Stomatology
**Zhengwei Xie**
Peking University Health Science Center
**Hao Liu** ( sdu2003@126.com )
Peking University School and Hospital of Stomatology: Peking University Hospital of Stomatology
https://orcid.org/0000-0002-5181-7024
**Yongsheng Zhou**
Peking University School and Hospital of Stomatology: Peking University Hospital of Stomatology
https://orcid.org/0000-0002-4332-0878

**Research Article**

**Keywords:** Ataluren, hBMMSCs, osteogenesis, osteoporosis, BMP-SMAD pathway

**Posted Date:** March 22nd, 2022

**DOI:** https://doi.org/10.21203/rs.3.rs-1427992/v1

# Abstract

Background

Both estrogen deficiency and aging may lead to osteoporosis. Developing novel drugs for treating osteoporosis is a popular research direction. Ataluren (ATA) is a nonaminoglycoside nonsense mutation inhibitor currently used clinically to treat muscular atrophy and Duchenne muscular dystrophy. However, little attention has been given to the role of Ataluren in osteogenesis, and it is unclear whether Ataluren can improve osteogenic differentiation of human- derived bone marrow mesenchymal stem cells (hBMMSCs) and treat osteoporosis.

Methods

In this study, we screened several potential therapeutic agents through a new deep learning-based efficacy prediction system (DLEPS) using transcriptional profiles for osteoporosis. We used ovariectomized (OVX) and aged female C57BL6 mice as bone loss models to demonstrate the role of preventing bone loss for Ataluren. The osteogenic differentiation of hBMMSCs was verified via qRT–PCR, staining and quantification of alkaline phosphatase and alizarin red S, and western blotting (WB), with and without an inhibitor of the BMP-SMAD signaling pathway and siBMP2.

Results

DLEPS screening led to a potential novel drug examinee, ataluren, for treating osteoporosis. Ataluren significantly reversed bone loss in ovariectomized mice. Next, ataluren significantly increased human bone marrow-derived mesenchymal stem cell (hBMMSC) osteogenic differentiation without cytotoxicity, indicated by the high expression index of osteogenic differentiation genes (*OCN*, *BGLAP*, *ALP*, *COL1A*, *BMP2*, *RUNX2*). Mechanistically, ataluren exerted its function through the BMP–SMAD pathway. Furthermore, it activated SMAD phosphorylation but osteogenic differentiation was attenuated by BMP2–SMAD inhibitors or small interfering RNA of *BMP2*. Finally, ataluren significantly reversed bone loss in aged mice.

Conclusions

In summary, our findings suggest that the DLEPS-screened ataluren may be a therapeutic agent against osteoporosis by aiding hBMMSC osteogenic differentiation.


# Background

Osteoporosis is a prevalent bone loss disease caused by a disruption in the balance between bone formation and bone resorption that eventually brings about bone loss (1). Currently, doctors mainly use osteoclast-inhibiting drugs to treat osteoporosis. The main categories are estrogens, bisphosphonates, and calcitriol, which favor the maintenance of bone mass by inhibiting osteoclasts (2, 3). However, these agents also cause adverse effects that limit their long-term use in osteoporotic patients, such as

osteonecrosis of the jaw, and breast and uterine cancer (4, 5). Decreasing bone resorption in patients with severe bone loss is insufficient for remedying their condition. There are few commercially available osteogenic drugs, including parathyroid hormones (PTHs). PTH affects bone remodeling by improving osteoblast proliferation and reducing apoptosis (6). However, in vivo osteogenesis peaks after 6–12 months of PTH analog therapy, after which the serum markers of osteoclast and osteoblast activity gradually return to baseline levels. This diminished osteoblast influence is one of the factors limiting the long-term clinical use of PTH analogs (7). The development of new osteogenic agents for enhancing osteogenesis is a popular research direction.

Big data and deep learning have provided a new avenue for drug discovery. Repurposing drug function can rapidly reduce drug development costs and meet clinical needs (8). The deep learning-based efficacy prediction system (DLEPS) is derived from Connectivity Map (CMAP), a web-based tool for screening compounds against various diseases using gene signatures (9, 10). This screening is attributed to comparing the DLEPS-predicted dataset with a user-selected phenotypic gene signature of interest using a high-resolution and high-specificity pattern matching algorithm (9). The search results in a series of compounds with gene expression patterns correlating highly with the phenotype of interest and ranked according to the gene set enrichment score, which aids the search for new disease therapeutic agents or therapeutic targets.

In the present study, we used the gene signatures of osteoporosis from ArrayExpress, a public database for microarrays and high-throughput sequencing data. We identified ataluren as a potential agent for treating osteoporosis. Ataluren is a protein expression repair drug for treating muscle atrophy and dystrophy (11)that was ratified by the European Commission in 2014. It affects the ribosomal translation of early termination codon mRNA and its advantages include minimal adverse effects and long-term use in patients aged ≥ 5 years (12–14).However, its function in bone stabilization has not been discovered.

Generally, mesenchymal stem cells (MSCs) can differentiate toward osteogenic, chondrogenic, and lipogenic lineages (15). MSC differentiation into osteoblasts can be promoted by activating osteogenic differentiation signaling pathways. The activation of various classical signaling pathways, such as that for Wnt–β-catenin (16), bone morphogenetic proteins (BMPs) (17–19) and Notch (20), upregulates the expression of transcription factors such as RUNX family transcription factor 2(RUNX2) and Sp7 transcription factor(OSX), which in turn activate alkaline phosphatase (ALP) and osteocalcin (OCN) and promote mineralization (21–26). However, it remains unknown whether ataluren can influence bone marrow-derived MSC (BMMSC) function via the osteogenic signaling pathway.

Therefore, in the present study, we evaluated the role of ataluren in reversing bone loss in ovariectomized (OVX) mice and explored its effects and underlying mechanisms on human BMMSC (hBMMSC) osteogenesis towards differentiation in vitro. Moreover, we used aged mouse models to measure the therapeutic effects of age-related bone loss in-depth.

# Methods

### Data Collection

Microarray database reference datasets were downloaded from the ArrayExpress database (accession number E-GEOD-35959; available from https://www.ebi.ac.uk/arrayexpress/experiments/E-GEOD-35959) by searching for osteoporosis, for which we obtained the gene expression profiles of 19 human MSC lines.

### Drug Repositioning

DLEPS was used for calculating the anti-osteoporosis score using the differentially expressed genes (DEG) described earlier. The drug with the lowest or highest score was likely to be effective for the selected disease, i.e., osteoporosis.

### Culture, osteogenic induction of hBMMSCs

Primary hBMMSCs were acquired from ScienCell and cultivated in PM [α-minimum essential medium (α-MEM, Gibco) containing 10% (v/v) fetal bovine serum (FBS, ExCell Bio) and 1% (v/v) penicillin streptomycin (Gibco)]. The osteogenic differential induction medium (OM) contained α-MEM with 10% (v/v) FBS, 1% (v/v) penicillin streptomycin, 10 nM dexamethasone (Sigma), 200 μM vitamin C (Sigma), and 10 mM β-glycerophosphate (βGP, Sigma).

### Concentrated Ataluren solution preparation

Chemical Structure:

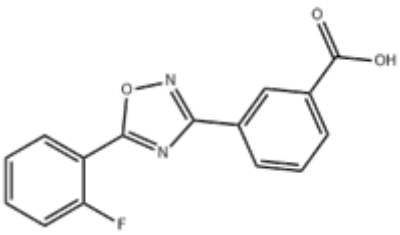


Ataluren (CSNpharm) was dissolved in DMSO (Sigma) and α-MEM to yield a concentrated solution of 0.1 mM. This was divided and used to detect the role of gradient concentrations of ataluren on hBMMSC differentiation and to select the best concentration for promoting osteoblastic differentiation.

### Cytotoxicity

The cytotoxicity of ataluren was determined by the CCK-8 assay. Briefly, cells were inoculated at 2,000 cells/well in clear, flat-bottomed, 96-well plates. Cells were then cultured in PM, or in PM at 10, 50 and 100 μM ataluren. cells from three wells of the same treatment were tested daily from day 1 to day 7 to determine the cytotoxicity of the relevant reagents by the CCK-8 assay. The cultures were then removed from the incubator and the absorbance at 570 nm was read.

### Staining and quantification of alkaline phosphatase (ALP) and alizarin red S (ARS)

Early markers of osteoblast differentiation were examined with ALP staining and quantitative determination of ALP activity. Late markers of osteoblast differentiation were examined using ARS staining and semi-quantitative determination of mineralization. ALP staining was performed using an NBT/BCIP staining kit (CoWin Biotech) according to the manufacturer's guidelines on day 7 after OM induction. ALP activity was tested with an ALP assay kit (Nanjing Jiancheng Bioengineering Institute). The ALP activity was calculated based on the absorbance in 520mm.

Fourteen days after OM induction, the cells were stained with 2% ARS buffer (Sigma). Mineral accumulation was quantified using 100 mM cetylpyridine solution (Sigma) in a multi-well sample plate. Mineral accumulation was quantitated based on the absorbance in 490mm.

### Western blot analysis

The hBMMSCs were cultured in 60-mm dishes and incubated with 1× radioimmunoprecipitation assay lysis buffer (Huaxingbio) containing a mixture of PMSF (Huaxingbio) and protease inhibitor (Huaxingbio). After centrifugation on ice, the protein concentration in the supernatant was measured by the bicinchoninic acid approach. The same amount of protein was split on a 10% sodium dodecyl sulfate–polyacrylamide gel and transferred onto a PVDF membrane (Millipore). The membranes were incubated in rapid blocking solution to block nonspecific binding, then incubated with primary antibodies against BMP2, RUNX2, OSX, SMAD1, SMAD5, SMAD1/5 (Abcam), pSMAD1/5 (Cell Signaling Technology), or GAPDH (Abcam). Then, the membranes were incubated with the secondary antibody for 1 h. Finally, the immunoreacted protein bands were detected by enhanced chemiluminescence.

### Quantitative real-time PCR (qRT–PCR)

Total cellular RNA was extracted from the hBMMSCs with TRIzol (Invitrogen) according to the manufacturer instruction manual. Complementary DNA (cDNA) was reverse-transcribed using a PrimeScript RT Reagent Kit (Takara). qRT-PCR was performed with SYBR Green Master Mix (YEASEN) on an ABI Prism 7500 RT-PCR System. The gene index was standardized to the *GAPDH* index, which was used as the housekeeping gene. The primer sequences used are presented in Additional file 1: TableS1. Each sample was taken in triplicate and fluorescence data was collected at the end of each cycle.

### Small interfering RNA (siRNA) transfection

BMP2-targeting siRNAs and Scramble siRNA were acquired from Sangon Biotech. The siRNA sequences were as follows: sense, GAUCAUCUGAACUCCACUAAUTT and antisense, AUUAGUGGAGUUCAGAUGAUCTT. 24 hours prior to treatment, hBMMSCs were inoculated at 80,000 cells/well in 24-well plates. Cells were treated with siBMP2 or scramble in 300 μL of Opti-MEM (Gibco) containing 1 μL of lipo-2000 (Invitrogen) for 4 hours. Thereafter the medium was changed to PM. The cells were transfected with siBMP2 and harvested for RNA analyses and western blotting after 2 days. For osteogenic induction, the cells were transfected every 5 days in OM and harvested after 1 week.

### Animals and experimental design and ethical statement

Female C57BL/6 mice were obtained from Charles River Laboratory Animal Technology Co., Ltd. They were housed in specific pathogen-free conditions at the Animal Center of Peking University School and Hospital of Stomatology. This study was authorized by the Peking University School of Medicine Institutional Committee for Animal Care and Use (LA2021040).

In vivo metabolism studies of ataluren suggested that the administration of ataluren in mice was by gavage at a concentration of 20mg/mL and a gavage dose of 15 mL/kg. Based on a mouse weight of 24 to 34 g, we can calculate the administered dose as 300 mg/kg(27).

Estrogen deficiency-induced bone loss model for primary validation  Twenty-five mice (56 days old) were placed in five groups(n = 5). After general anesthesia, bilateral OVX or sham surgery was performed with standardized techniques. Four weeks after surgery, 300 mg/kg/d ataluren (20 mg/mL, Macklin) mixed in 0.5% Carboxymethylcellulose (CMC, Sigma), 36.4 mg/kg/d natamycin (NATA, 15 mg/mL, Solarbio) mixed in 0.5% CMC and 0.26 mg/kg/d prucalopride (PRU, 0.0173 mg/mL, Mitachieve) mixed in 0.5% CMC was administered by gavage for 2 months (once every other day). The five groups were: (1) SHAM+CMC, (2) OVX+CMC, (3) OVX+ATA, (4) OVX+NATA, and (5) OVX+PRU.

Estrogen deficiency-induced bone loss model: Twenty mice (56 days old) were placed in four groups (n = 5). Four weeks after OVX or sham surgery, 300 mg/kg/d ataluren mixed in 0.5% CMC was administered by gavage for 2 months (once every other day). The four groups were: (1) SHAM+CMC, (2) SHAM+ATA, (3) OVX+CMC, and (4) OVX+ATA.

Age-related bone loss model: Ten mice (18 months old) were stochastically divided into two groups (n = 5): (1) Aged+CMC and (2) Aged+ATA. 300 mg/kg/d ataluren (20 mg/mL, Macklin) mixed in 0.5% CMC (Sigma) was administered by gavage for 2 months (once every other day).

All mice were euthanized, and the left femur and vital internal organs were collected and fixed in 10% formalin. The right femur was also collected and preserved from light. The serum was also collected from each mouse. The major organs were carefully collected and fixed in 10% formalin for H&E staining of tissue sections to observe the tissue toxicity of ataluren.

### Serum enzyme-linked immunosorbent assay (ELISA)

Serum PINP and serum CTX-1 were used as markers of bone formation and bone resorption, respectively. The serum biomarkers were tested using an ELISA kit (Jiangsu Meimian Industrial Co., Ltd.).

### Bone histomorphology

Bone histomorphology analyses were performed according to a previously described protocol(28). For the measurement of dynamic bone parameters, the mice were injected with calcium xanthophyll green (10 mg/kg body weight) and alizarin complexes (10 mg/kg body weight) at 7 and 2 days before euthanasia, respectively. After euthanasia of the mice, the right femur was removed and stored away from light, dehydrated, and embedded for hard tissue sectioning. The double-labeling in the bone tissue was

observed under fluorescence microscopy, and quantitative analysis was performed using Image J (National Institutes of Health). MAR (mineral apposition rates) represents the rate of new bone formation.

The left femurs were carefully collected and fixed in 10% formalin, dehydrated in 70% ethanol and embedded in methyl methacrylate. The femur was cut in half at the mid-axis and sectioned in the transverse plane of a 200 μm thick section for H&E staining and observed under the microscope.

### Micro-computed tomography

Femoral specimens were scanned with the Inveon MM System (Siemens) micro-computed tomographer. The scanning conditions were 60 kV, 500 μA, and precision of 8.82 μm. Parametric analysis was performed using Inveon Research Workplace software (Siemens). The measurement area was 1 mm proximal to the epiphysis. The parameters analyzed were bone mineral density (BMD), bone volume/total volume (BV/TV), bone surface area/bone volume (BS/BV), trabecular thickness (Tb.Th), trabecular number (Tb.N), and trabecular separation (Tb.Sp) by Inveon Research Workplace (Siemens).

### Statistical analysis

All data are expressed as the mean ± standard deviation (SD) of at least 3 experiments per group. The statistics were analyzed with the Student t-test or one-way analysis of variance (ANOVA) via SPSS 23.0 (SPSS Inc.). $P < 0.05$ and $<0.01$ indicated statistical significance.

## Results

### Ataluren prevents bone loss in OVX mice

First, we identified the up-/down-regulated genes of primary osteoporosis and advanced age on human MSCs (E-GEOD-35959) (29) (see Additional file 2: TableS2 for the list of genes). Then, the up-/down-regulated genes were used as DLEPS input (REF https://www.nature.com/articles/s41587-021-00946-z) to calculate the efficacy score using the D3680 library (Additional file 3: TableS3). We identified many small molecules that could yield new ideas for therapeutic research on osteoporosis. The results of the DLEPS screening are shown in the scatter plot (Fig. 1a), the top points in the ranking of the effective scores for osteoporosis are concentrated in the upper right corner. The scores of the top-ranked compounds for osteoporosis therapy are shown in a heat map (Fig. 1b). We excluded the compounds with reported osteoporosis therapeutic effects and toxic side effects through a literature search. Ataluren was ranked second, while tideglusib, coumarin, and dydrogesterone promote the regeneration of bone defects(30–32). Zoxazolamine and phenacetin have considerable biological toxicity, limiting their clinical application (33, 34).

Ataluren (ATA), natamycin (NATA), and prucalopride (PRU) were selected for micro-computed tomography (micro-CT) examination of whether they can reverse bone loss in OVX mice. Supplementary Figure S1a shows representative micro-CT and hematoxylin–eosin (H&E) staining images of OVX mouse femur. Ataluren improved bone mineral density (BMD) and bone microarchitecture comparable to that of the

SHAM + CMC (carboxymethyl cellulose) group and was superior to that of the natamycin and prucalopride groups (Additional file 4: Figure S1). Our results show that among the three drug candidates, ataluren induced the best reversal of bone loss in the OVX mice. Therefore, ataluren was selected for further study.

To confirm the effect of ataluren on inhibiting bone loss, we compared the morphological and H&E staining images of the femur and bone morphological parameters in four groups of mice (8 months old): SHAM + CMC (sham surgery plus gavage CMC, n = 5), SHAM + ATA (sham surgery plus gavage ataluren, n = 5), OVX + CMC (OVX surgery plus gavage CMC, n = 5), and OVX + ATA (OVX surgery plus gavage ataluren, n = 5) (Fig. 1c). The OVX + ATA mice had higher BMD, bone volume/total volume (BV/TV), trabecular thickness (Tb.Th), and trabecular bone number (Tb.N) ($p < 0.01$, $p < 0.01$, $p < 0.05$, $p < 0.01$, respectively) and lower trabecular spacing (Tb.Sp) compared with the OVX + CMC group ($p < 0.01$) (Fig. 1d). New bone formation in the distal femoral epiphysis was evaluated by dual labeling with calcium xanthophyll green and alizarin complexes. There was greater MAR (mineral apposition rates) in the OVX + ATA mice compared to the OVX + CMC mice ($p < 0.01$) (Fig. 1d, 1f), indicating that ataluren promoted bone formation. Additionally, ataluren significantly increased levels of the serum bone formation marker PINP (propeptide of type I collagen) ($p < 0.05$) (Fig. 1g) and decreased levels of the bone resorption marker CTX-1 (C-terminal telopeptide of type I collagen) ($p < 0.05$) (Fig. 1h). Although PINP was increased in OVX mice, their CTX-1 values were also significantly increased, indicating that the imbalance in bone metabolism was more severe in OVX mice. These results demonstrate that ataluren significantly recovers bone loss with better trabecular structure and higher bone volume in OVX mice.

**Ataluren promotes hBMMSC osteogenic differentiation in vitro**

We used hBMMSCs as a model system for uncovering the potential effects of ataluren on bone formation. We examined ataluren cytotoxicity by using the Cell Counting Kit-8 (CCK-8) assay to examine its effects on hBMMSC proliferation. The CCK-8 curves showed that, from day 4–7, cells treated with 1‰ dimethyl sulfoxide (DMSO) and 10 μM and 50 μM ataluren showed no significant difference in cell proliferation capacity compared with cells treated with proliferation medium (PM) (Additional file 5: Figure S2a). Cell proliferation capacity was partially inhibited by 100 μM ataluren, indicating safe usage under 50 μM.

The effect of ataluren on hBMMSC osteogenic differentiation was determined using ALP and alizarin red S (ARS) staining and quantitative analysis. Ataluren (10, 50, and 100 μM) increased ALP activity compared with the OM (osteogenic medium) group ($p < 0.05$, Fig. 2a, 2b), peaking at 50 μM. ARS staining showed that 10 and 50 μM ataluren increased mineralized nodules in the hBMMSCs as compared with the OM group (both, $p < 0.05$) and also peaked at 50 μM (Fig. 2c, 2d). Furthermore, the mRNA expression levels of RUNX2, an osteogenic differentiation marker, were significantly increased in hBMMSCs treated with 10 and 50 μM ataluren ($p < 0.01$, Fig. 2e). Western blotting showed that 10 and 50 μM ataluren significantly elevated RUNX2 and OSX protein levels as compared with that in the OM group ($p < 0.01$, Fig. 2f, 2g). However, the addition of ataluren to the PM did not promote hBMMSC osteogenic

differentiation. Moreover, the addition of 1‰ DMSO to the PM or OM had no promoting effects on osteogenesis (Additional file 5: Figure S2b).

## Ataluren promotes hBMMSC osteogenic differentiation through BMP–SMAD signaling pathway activation

We performed RNA sequencing (RNA-seq) on ataluren-treated hBMMSCs to systematically examine how it affects global transcriptional changes. Ataluren (50 μM) upregulated 199 genes and downregulated 169 genes compared to the OM group (Fig. 3a). Among the upregulated genes, the most significantly expressed gene was *DUSP5* ($p < 0.001$) (Fig. 3b). *DUSP5* has been suggested to enhance MSC osteogenic differentiation through the BMP–SMAD pathway (Liu et al., 2021). Kyoto Encyclopedia of Genes and Genomes (KEGG) pathway analysis showed the most significant enrichment in the transforming growth factor beta (TGF-β) signaling pathway (Fig. 3c). Similarly, gene ontology (GO) enrichment analysis showed enrichment of the BMP signaling pathway (Fig. 3d). TGF-β–BMP signaling can converge on the *Runx2* gene via a classical SMAD-dependent pathway to control MSC precursor cell differentiation and promote bone formation (M. Wu, Chen, & Li, 2016; Zou et al., 2021). Accordingly, we hypothesized that ataluren promotes osteogenesis by activating the BMP–SMAD pathway. To understand the potential molecular mechanisms by which ataluren promotes hBMMSC differentiation into osteoblasts, BMP–SMAD signaling pathway activation was investigated by quantitative real-time PCR (qRT-PCR) and western blotting. The qRT-PCR results demonstrated that 50 μM ataluren remarkably increased the mRNA expression levels of *BMP2*, *COL1A*, *ALP*, *BGLAP*, and *OSX* compared with OM (all, $p < 0.05$) (Fig. 3e). Moreover, it activated genes downstream of the SMAD signaling pathway during osteogenesis in hBMMSCs (Fig. 3f). That is, ataluren upregulated phosphorylated (p)*SMAD1/5*, *RUNX2*, *OSX*, and *BMP2* ($p < 0.01$, $p < 0.05$, $p < 0.05$, and $p < 0.01$, respectively, Fig. 3g).

## Inhibition of the BMP–SMAD pathway blocks ataluren-induced hBMMSC osteogenic differentiation

We blocked BMP–SMAD signaling with the TGF-β–SMAD inhibitor LDN-193189 HCl and used small interfering RNA (siRNA)-mediated gene silencing targeting *BMP2* (siBMP2) to verify if ataluren regulates osteoblast differentiation via BMP–SMAD. The increased ALP activity was blocked after BMP–SMAD had been inhibited by siBMP2 and LDN-193189 HCl (both, $p < 0.01$) (Fig. 4a, 4c). The increase in calcium nodules, measured by ARS staining, was also blocked by LDN-193189 HCl and siBMP2 as compared with the 50 μM ataluren treatment group or the Scramble + 50 μM ataluren group (both, $p < 0.01$) (Fig. 4b, 4d). Western blotting and quantification showed that the increase in SMAD1/5 phosphorylation (both, $p < 0.01$) and the osteogenic markers BMP2 (both, $p < 0.01$) and RUNX2 (both, $p < 0.01$) was inhibited in the presence of LDN-193189 HCl, siBMP2, or both (Fig. 4e, 4f). These results confirm that ataluren induced a positive osteogenic promoting effect in hBMMSCs through the BMP–SMAD pathway.

## Ataluren partially reverses bone loss in aged mice

It is important to know if ataluren is effective in naturally aged mice. We treated 18-month-old mice with ataluren and measured their bone mass and bone density by micro-CT. Ataluren significantly increased

BV/TV and Tb.Th (both, $p < 0.01$) and decreased Tb.Sp ($p < 0.01$) as compared with the Aged + CMC mice (Fig. 5a, 5c). MAR was visualized with calcium xanthophyll green and alizarin complexes. As expected, the new bone formation rate was meager in the control aged mice. In contrast, the ataluren-treated mice had greatly restored new bone formation capability ($p < 0.01$) (Fig. 5b, d). Furthermore, ataluren treatment significantly increased PINP levels ($p < 0.05$) (Fig. 5e) and decreased CTX-1 levels ($p < 0.05$) (Fig. 5f). These results indicate that ataluren can reverse bone loss in aged mice.

To explore the safety of ataluren, we treated sham control mice (8 weeks) and aged mice with 20 mg/mL ataluren for 2 months. There were no toxic side effect changes in the heart, spleen, liver, lungs, or kidneys of the ataluren-treated mice (Additional file 6: Figure S3).

# Discussion

In the present study, the underlying anti-osteoporotic effect of ataluren was predicted by a DLEPS. Experimentally, ataluren restored OVX-related bone loss. It promoted hBMMSC osteogenic differentiation dependent on the BMP–SMAD pathway. This study validated ataluren reversal of bone loss in aged mice.

Currently, drug-related research and development benefit from advances in biotechnology and computer technology. Different algorithms, software, and tools continue to emerge from the analysis and summary of large amounts of experimental data. The gene expression profiles in disease reveal potential changes in gene activity that contribute to illness and enable targeted therapeutic interventions (35–37). In the present study, we examined the gene expression profiles of human MSCs from the ArrayExpress database for senescence (GSE35956), primary osteoporosis (GSE35957), and cellular senescence (GSE35958). Then, we used DLEPS to identify small bioactive molecules capable of reversing the genetic changes in osteoporosis.

As shown in Fig. 1c (ct.BMD, BV/TV, Tb.N), Fig. 1f (MAR) and Fig. 1g, ataluren increases bone mass by increasing bone formation, even in untreated mice (SHAM + ATA vs SHAM + CMC). This suggests that ataluren may be a drug that promotes bone formation, and we therefore subsequently explored primarily the osteogenic to differentiation effects of ataluren on hBMMSCs. Furthermore, the fact that ataluren improved bone formation in both young and old animals suggests that the efficacy of ATA is not age-dependent.

During protein integration, nonsense mutations in the premature termination codon produce a truncated, inactive protein product. This defective gene product causes many diseases, including muscular dystrophy, cystic fibrosis, and some cancers (38–40). Ataluren is a small-molecule nonsense repressor that stimulates stop codon reading and thereby acts as a treatment for these diseases (41). The addition of Stop-POST5 (containing the UGA stop codon at the A-site) is shifted to extension. Ataluren cannot provoke foundational read-through in eRF1/eRF3 deficiency (42). A likely target of ataluren is the ribosome, which produces full-length proteins by facilitating the insertion of near-homologous tRNAs at nonsense codon sites, with no apparent effect on transcription, mRNA processing, or mRNA or protein stability (43). here is little direct evidence that ataluren promotes hBMMSC osteogenic differentiation.

Only one study has shown that ataluren can treat mucopolysaccharidosis type VI, whose clinical characteristic is multiple bone dysplasia, by restoring arylsulfatase B deficiency and improving treatment effectiveness in areas such as bone or cartilage (44). Taken together, this evidence suggests that ataluren may act in the targeted management of hBMMSC osteogenic differentiation.

Furthermore, the transcriptome sequencing analysis results showed that 50 μM ataluren upregulated DUSP5 most significantly, which elevated MSC osteogenic differentiation through the BMP–SMAD pathway, as demonstrated by our group previously (45). It was also suggested that DUSP5 overexpression inhibits NF-κB pathway activation and thereby controls inflammation (46). This may partly explain the decreased CTX-1 in the serum of OVX + ATA and Aged + ATA mice. Based on this, we hypothesized that ataluren promotes osteogenesis by activating the BMP–SMAD pathway. Exploration of the osteogenesis mechanisms showed that ataluren upgrades osteogenic differentiation by activating the BMP–SMAD signaling pathway. BMP2, a BMP family member, facilitates osteoblast differentiation by raising endocellular ALP activity and OCN and collagen synthesis and differentiation (47). BMPs produce their effects by interacting with two BMP receptors (BMPRs). BMPRs exert their effects by interacting with extracellular BMPRs. BMPRs are activated by binding to extracellular BMP molecules (48, 49). A recent study demonstrated that 28.4 μg/mL ataluren improved BMPR2 protein expression in the R584X animal model and sectionally restored the BMPR2 protein index in endothelial cells extracted from patients carrying the R584X mutation (50). In a study of hereditary pulmonary hypertension, western blotting of endothelial cell lysates treated with 5.7 μg/mL ataluren demonstrated 1.9- and 3.7-fold augmentation in BMPR2 protein expression and ligand-dependent phosphorylation of the downstream target gene SMADs, respectively (51). Therefore, our results are consistent with previous reports. Nevertheless, our study indicates for the first time that ataluren facilitates osteogenesis via the BMP–SMAD signaling pathway. Although the mechanism of ataluren in promoting hBMMSC osteogenesis has not been clarified, it is mediated, at least in part, through BMP–SMAD signaling pathway activation.

Nonetheless, our study has some limitations. First, the results of both in vivo experiments (OVX and aging studies) indicated a reduction of bone resorption as evidenced by reduced CTX-1 levels. However, given that ataluren may be a pro-synthetic drug, we have not further determined the effect of ataluren on osteoclast differentiation and function, which warrants further exploration in future studies. Second, we did not determine the effect of ataluren on in vitro osteogenesis as studied by overexpression. Finally, We infer that the mechanism of increased bone formation in ataluren is activation of the BMP signaling pathway in hBMMSCs based on the results of in vitro experiments, which need to be further validated by in vivo intervention-based experiments.

# Conclusion

In conclusion, our results suggest that DLEPS screening can identify new drug candidates for remedying osteoporosis. The screening representative compound ataluren prevented OVX-induced bone loss. Ataluren promoted osteogenic differentiation by increasing hBMMSC ALP activity and mineralization levels and increasing the mRNA and protein expression of osteogenic markers. Moreover, ataluren

prevented bone loss caused by age-related conditions in mice. Mechanistically, ataluren promoted osteogenesis by activating the BMP–SMAD signaling pathway. Our study suggests that ataluren may be a therapeutic agent against osteoporosis by aiding hBMMSC osteogenic differentiation (Fig. 6).

# Abbreviations

ALP Alkaline phosphatase

ARS Alizarin red S

ATA Ataluren

BGLAP Bone gamma-carboxy glutamic acid-containing protein

BMD Bone mineral density

BMMSCs Bone marrow mesenchymal stem cells

BV/TV Trabecular bone volume/tissue volume

BMP bone morphogenetic proteins

CMAP Connection Map

CMC Carboxymethyl Cellulose

DMSO Dimethyl sulfoxide

ELISA Enzyme-linked immunosorbent assay

ECL enhanced chemiluminescence

GAPDH Glyceraldehyde 3-phosphate dehydrogenase

H&E Hematoxylin and eosin

hBMMSCs human bone marrow mesenchymal stem cells

Micro-CT Microcomputed tomography

MSCs mesenchymal stem cells

MAPK mitogen-activated protein kinase

OCN Osteocalcin

OM Osteogenic medium

OVX ovariectomized

P1NP Procollagen I N-terminal propeptide

PM Proliferation medium

PTH parathyroid hormones

qRT–PCR Quantitative reverse transcription PCR

RUNX2 Runt-related transcription factor 2

siRNA small interfering RNA

Tb. N Trabecular number

Tb. Sp Trabecular spacing

Tb. Th Trabecular thickness

βGP β-glycerophosphate

# Declarations


### Funding

This work was supported by grants from the National Natural Science Foundation of China [grant numbers 81700935, 81870742] and the Beijing Natural Science Foundation [L182006].


### Availability of data and materials

The authors confirm that all data underlying the findings are fully available.

### Ethics approval and consent to participate

This study was carried out in strict accordance with the recommendations of the Guide for the Care and Use of Laboratory Animals of the National Institutes of Health. The protocol was approved by the Institutional Animal Care and Use Committee of the Peking University Health Science Center (approval no. LA2021040). All surgeries were performed under anesthesia, and efforts were made to minimize animal suffering.

### Competing interests

The authors declare that they have no competing interests.

### Consent for publication

Not applicable

### Authors' contributions

LZ was responsible for the conception and design, collection and assembly of data, analysis and interpretation, and manuscript writing. GR was responsible for the collection and assembly of data and data analyses and interpretation in animal experiments. YS and YZ were responsible for the collection and assembly of data and data analyses in the molecular biology experiments. YZ, HL and ZX were accountable for the conception and design, financial support, and manuscript writing. All authors read and approved the final manuscript.

## References


1. Aspray TJ, Hill TR. Osteoporosis and the Ageing Skeleton. Subcell Biochem. 2019;91:453-76.
2. Langdahl B. Treatment of postmenopausal osteoporosis with bone-forming and antiresorptive treatments: Combined and sequential approaches. Bone. 2020;139:115516.
3. Eriksen EF, Halse J, Moen MH. New developments in the treatment of osteoporosis. Acta Obstet Gynecol Scand. 2013;92(6):620-36.
4. Feller L, Wood NH, Khammissa RA, Chikte UM, Bouckaert M, Lemmer J. Bisphosphonate-related osteonecrosis of the jaw. Sadj. 2011;66(1):30-2.
5. Migliorati CA, Siegel MA, Elting LS. Bisphosphonate-associated osteonecrosis: a long-term complication of bisphosphonate treatment. Lancet Oncol. 2006;7(6):508-14.
6. Tay D, Cremers S, Bilezikian JP. Optimal dosing and delivery of parathyroid hormone and its analogues for osteoporosis and hypoparathyroidism - translating the pharmacology. Br J Clin Pharmacol. 2018;84(2):252-67.
7. Leder BZ. Parathyroid Hormone and Parathyroid Hormone-Related Protein Analogs in Osteoporosis Therapy. Curr Osteoporos Rep. 2017;15(2):110-9.
8. Qu XA, Rajpal DK. Applications of Connectivity Map in drug discovery and development. Drug Discov Today. 2012;17(23-24):1289-98.
9. Zhu J, Wang J, Wang X, Gao M, Guo B, Gao M, et al. Prediction of drug efficacy from transcriptional profiles with deep learning. Nature biotechnology. 2021;39(11):1-9.
10. Jiang H, Hu C, Chen M. The Advantages of Connectivity Map Applied in Traditional Chinese Medicine. Front Pharmacol. 2021;12:474267.
11. Bushby K, Finkel R, Wong B, Barohn R, Campbell C, Comi GP, et al. Ataluren treatment of patients with nonsense mutation dystrophinopathy. Muscle Nerve. 2014;50(4):477-87.
12. Hirawat S, Welch EM, Elfring GL, Northcutt VJ, Paushkin S, Hwang S, et al. Safety, tolerability, and pharmacokinetics of PTC124, a nonaminoglycoside nonsense mutation suppressor, following single- and multiple-dose administration to healthy male and female adult volunteers. J Clin Pharmacol. 2007;47(4):430-44.

13. Campbell C, Barohn RJ, Bertini E, Chabrol B, Comi GP, Darras BT, et al. Meta-analyses of ataluren randomized controlled trials in nonsense mutation Duchenne muscular dystrophy. J Comp Eff Res. 2020;9(14):973-84.
14. Berger J, Li M, Berger S, Meilak M, Rientjes J, Currie PD. Effect of Ataluren on dystrophin mutations. J Cell Mol Med. 2020;24(12):6680-9.
15. Short B, Brouard N, Occhiodoro-Scott T, Ramakrishnan A, Simmons PJ. Mesenchymal stem cells. Arch Med Res. 2003;34(6):565-71.
16. Baron R, Kneissel M. WNT signaling in bone homeostasis and disease: from human mutations to treatments. Nat Med. 2013;19(2):179-92.
17. Thielen NGM, van der Kraan PM, van Caam APM. TGFβ/BMP Signaling Pathway in Cartilage Homeostasis. Cells. 2019;8(9):69-99.
18. Hettiaratchi M, Krishnan L, Rouse T, Chou C, McDevitt T, Guldberg R. Heparin-mediated delivery of bone morphogenetic protein-2 improves spatial localization of bone regeneration. Science advances. 2020;6(1):eaay1240.
19. Chen G, Deng C, Li YP. TGF-β and BMP signaling in osteoblast differentiation and bone formation. Int J Biol Sci. 2012;8(2):272-88.
20. Tezuka K, Yasuda M, Watanabe N, Morimura N, Kuroda K, Miyatani S, et al. Stimulation of osteoblastic cell differentiation by Notch. J Bone Miner Res. 2002;17(2):231-9.
21. Milat F, Ng KW. Is Wnt signalling the final common pathway leading to bone formation? Mol Cell Endocrinol. 2009;310(1-2):52-62.
22. Katagiri T, Watabe T. Bone Morphogenetic Proteins. Cold Spring Harb Perspect Biol. 2016;8(6).
23. Majidinia M, Sadeghpour A, Yousefi B. The roles of signaling pathways in bone repair and regeneration. J Cell Physiol. 2018;233(4):2937-48.
24. Lu J, Zhang H, Pan J, Hu Z, Liu L, Liu Y, et al. Fargesin ameliorates osteoarthritis via macrophage reprogramming by downregulating MAPK and NF-κB pathways. Arthritis Res Ther. 2021;23(1):142.
25. Ramasamy SK, Kusumbe AP, Wang L, Adams RH. Endothelial Notch activity promotes angiogenesis and osteogenesis in bone. Nature. 2014;507(7492):376-80.
26. Komori T. Regulation of bone development and extracellular matrix protein genes by RUNX2. Cell Tissue Res. 2010;339(1):189-95.
27. Kong R, Ma J, Hwang S, Goodwin E, Northcutt V, Babiak J, et al. Metabolism and Disposition of Ataluren after Oral Administration to Mice, Rats, Dogs, and Humans. Drug Metab Dispos. 2020;48(4):317-25.
28. Movérare-Skrtic S, Wu J, Henning P, Gustafsson KL, Sjögren K, Windahl SH, et al. The bone-sparing effects of estrogen and WNT16 are independent of each other. Proc Natl Acad Sci U S A. 2015;112(48):14972-7.
29. Benisch P, Schilling T, Klein-Hitpass L, Frey SP, Seefried L, Raaijmakers N, et al. The transcriptional profile of mesenchymal stem cell populations in primary osteoporosis is distinct and shows

overexpression of osteogenic inhibitors. PLoS One. 2012;7(9):e45142.

30. Lektemur Alpan A, Çalişir M, Kizildağ A, Özdede M, Özmen Ö. Effects of a Glycogen Synthase Kinase 3 Inhibitor Tideglusib on Bone Regeneration With Calvarial Defects. J Craniofac Surg. 2020;31(5):1477-82.
31. Lee EJ, Kang MK, Kim YH, Kim DY, Oh H, Kim SI, et al. Coumarin Ameliorates Impaired Bone Turnover by Inhibiting the Formation of Advanced Glycation End Products in Diabetic Osteoblasts and Osteoclasts. Biomolecules. 2020;10(7):52-62.
32. Stevenson JC, Teter P, Lees B. 17beta-estradiol (1 mg/day) continuously combined with dydrogesterone (5, 10 or 20 mg/day) increases bone mineral density in postmenopausal women. Maturitas. 2001;38(2):197-203.
33. Nahorski SR. The Pharmacological Basis of Therapeutics, 8th Edition. Trends in Pharmacological Sciences. 1990.
34. Saleem TH, Abo El-Maali N, Hassan MH, Mohamed NA, Mostafa NAM, Abdel-Kahaar E, et al. Comparative Protective Effects of N-Acetylcysteine, N-Acetyl Methionine, and N-Acetyl Glucosamine against Paracetamol and Phenacetin Therapeutic Doses-Induced Hepatotoxicity in Rats. Int J Hepatol. 2018;2018:7603437.
35. Yu G, Wang L, Li Y, Ma Z, Li Y. Identification of drug candidate for osteoporosis by computational bioinformatics analysis of gene expression profile. Eur J Med Res. 2013;18(1):5.
36. Brum AM, van de Peppel J, van der Leije CS, Schreuders-Koedam M, Eijken M, van der Eerden BC, et al. Connectivity Map-based discovery of parbendazole reveals targetable human osteogenic pathway. Proc Natl Acad Sci U S A. 2015;112(41):12711-6.
37. Zhao P, Mangleburg CG, Al-Ramahi I, Botas J, Shulman JM. Systems genetic dissection of Alzheimer's disease brain gene expression networks. Alzheimers Dement. 2021;17 Suppl 2:e058716.
38. Finkel RS. Read-through strategies for suppression of nonsense mutations in Duchenne/ Becker muscular dystrophy: aminoglycosides and ataluren (PTC124). J Child Neurol. 2010;25(9):1158-64.
39. Aslam AA, Higgins C, Sinha IP, Southern KW. Ataluren and similar compounds (specific therapies for premature termination codon class I mutations) for cystic fibrosis. Cochrane Database Syst Rev. 2017;1(1):Cd012040.
40. Porter JJ, Heil CS, Lueck JD. Therapeutic promise of engineered nonsense suppressor tRNAs. Wiley Interdiscip Rev RNA. 2021;12(4):e1641.
41. Kong R, Ma J, Hwang S, Moon YC, Welch EM, Weetall M, et al. In vitro metabolism, reaction phenotyping, enzyme kinetics, CYP inhibition and induction potential of ataluren. Pharmacol Res Perspect. 2020;8(2):e00576.
42. Ng MY, Li H, Ghelfi MD, Goldman YE, Cooperman BS. Ataluren and aminoglycosides stimulate read-through of nonsense codons by orthogonal mechanisms. Proc Natl Acad Sci U S A. 2021;118(2).
43. Roy B, Friesen WJ, Tomizawa Y, Leszyk JD, Zhuo J, Johnson B, et al. Ataluren stimulates ribosomal selection of near-cognate tRNAs to promote nonsense suppression. Proc Natl Acad Sci U S A. 2016;113(44):12508-13.

44. Bartolomeo R, Polishchuk EV, Volpi N, Polishchuk RS, Auricchio A. Pharmacological read-through of nonsense ARSB mutations as a potential therapeutic approach for mucopolysaccharidosis VI. J Inherit Metab Dis. 2013;36(2):363-71.
45. Liu X, Liu X, Du Y, Hu M, Tian Y, Li Z, et al. DUSP5 promotes osteogenic differentiation through SCP1/2-dependent phosphorylation of SMAD1. Stem Cells. 2021;39(10):1395-409.
46. Wu Z, Xu L, He Y, Xu K, Chen Z, Moqbel SAA, et al. DUSP5 suppresses interleukin-1β-induced chondrocyte inflammation and ameliorates osteoarthritis in rats. Aging (Albany NY). 2020;12(24):26029-46.
47. Wu M, Chen G, Li YP. TGF-β and BMP signaling in osteoblast, skeletal development, and bone formation, homeostasis and disease. Bone Res. 2016;4:16009.
48. Carreira AC, Alves GG, Zambuzzi WF, Sogayar MC, Granjeiro JM. Bone Morphogenetic Proteins: structure, biological function and therapeutic applications. Arch Biochem Biophys. 2014;561:64-73.
49. Sampath TK, Reddi AH. Discovery of bone morphogenetic proteins - A historical perspective. Bone. 2020;140:115548.
50. Long L, Yang X, Southwood M, Moore S, Crosby A, Upton PD, et al. Targeting translational read-through of premature termination mutations in BMPR2 with PTC124 for pulmonary arterial hypertension. Pulm Circ. 2020;10(3):2045894020935783.
51. Drake KM, Dunmore BJ, McNelly LN, Morrell NW, Aldred MA. Correction of nonsense BMPR2 and SMAD9 mutations by ataluren in pulmonary arterial hypertension. Am J Respir Cell Mol Biol. 2013;49(3):403-9.

# Figures

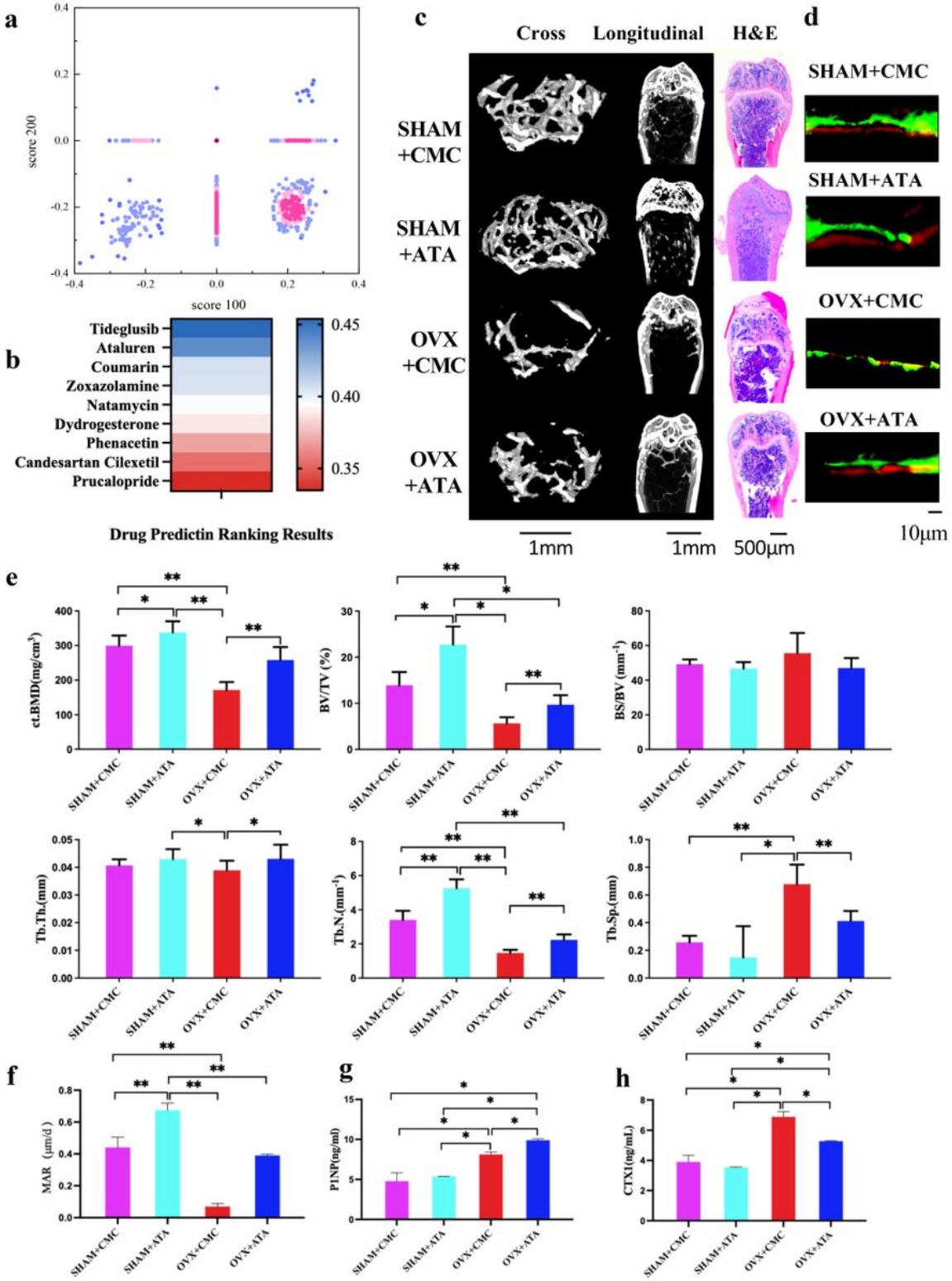


## Figure 1

Ataluren prevents bone loss in OVX mice. **a** Scatter plot of osteoporosis efficacy scores. The DLEPS made predictions based on osteoporosis differential genes, with the color gradient showing the density of the dots. **b** Heat map of the top nine predicted drugs. Ataluren was ranked second. **c** Micro-CT (left) and H&E (right) staining images of SHAM+CMC, SHAM+ATA, OVX+CMC, and OVX+ATA femurs. Micro-CT images are at a scale of 1 mm. H&E staining images are at a scale of 500 μm. **d** Representative images of new

bone formation in the distal femoral epiphysis assessed by double-labeling with calcein and alizarin-3-methyliminodiacetic acid. Scale bar, 10 μm. **e** Compared to CMC-treated OVX mice, ataluren-treated OVX mice had increased BMD, BV/TV, Tb.Th, and Tb.N and decreased Tb.Sp. **f** Mineral apposition rates (MAR) of SHAM+CMC, SHAM+ATA, OVX+CMC, and OVX+ATA. **g** Serum levels of PINP. **h** Serum levels of CTX-1. All data shown are the mean ± SD in **e f g h**, n=5. **P*< 0.05, ***P*< 0.01 by ANOVA.

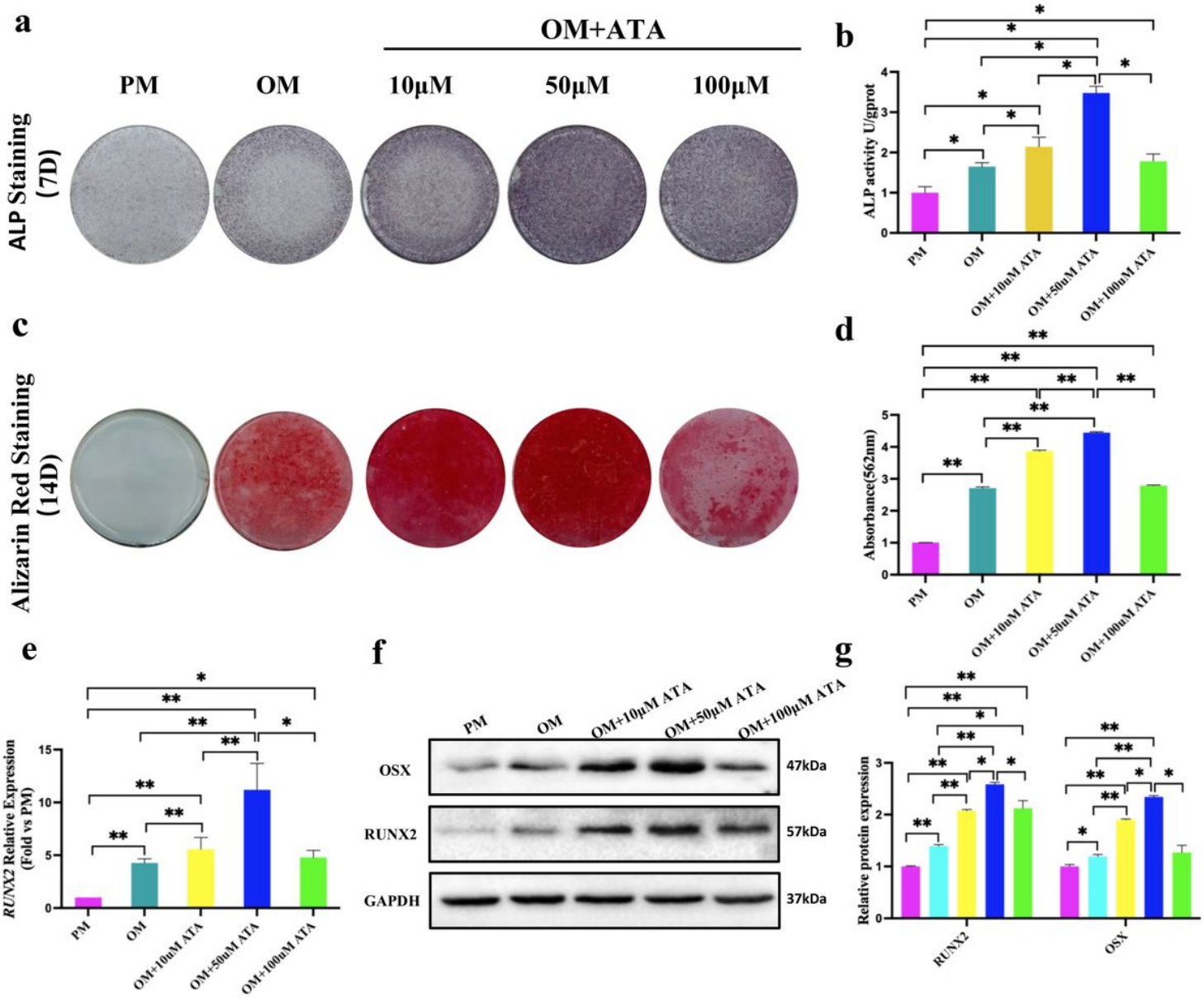


## Figure 2

Ataluren promotes hBMMSC osteogenic differentiation in vitro. **a** Ataluren (10, 50, 100 μM) improved hBMMSC ALP activity. **b** ALP activity quantification. **c** ARS staining showing that 10 and 50 μM ataluren increased hBMMSC mineralization while 100 μM ataluren decreased it. **d** ARS semi-quantification results were consistent with that of ARS staining. **e** qRT-PCR results for *RUNX2* after 7-day ataluren treatment. **f** Western blotting analysis of RUNX2, OSX, and the internal control GAPDH. **g** Quantitative analysis of

OSX/GAPDH and RUNX2/GAPDH. All data shown are the mean ± SD in **b d e g**, n=3. *$P$< 0.05, **$P$< 0.01 by ANOVA.

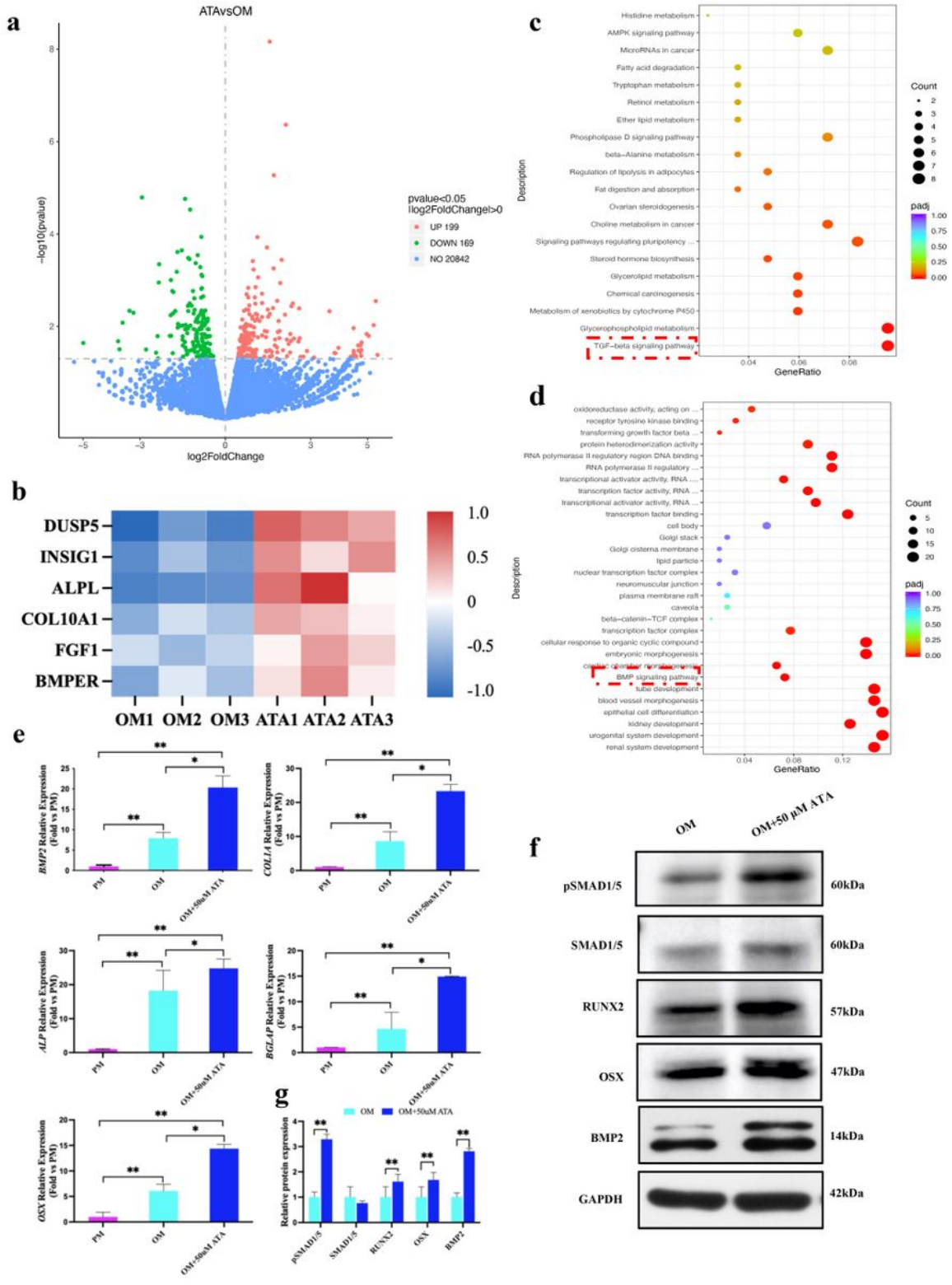


## Figure 3

Ataluren promoted hBMMSC osteogenic differentiation by activating the BMP–SMAD pathway. **a** Differential expression analysis results of RNA-seq data from hBMMSCs. **b** RNA-seq showing the

upregulated genes between the ATA and OM groups. *DUSP5* was significantly different. **c** KEGG pathway enrichment analysis of DEGs using DAVID. The gene ratio was measured as the genes enriched/total genes. **d** GO enrichment analysis of DEGs using DAVID. The gene ratio was measured as the genes enriched/total genes. **e** qRT-PCR showing that 50 μM ataluren promoted *BMP2*, *COL1A*, *ALP*, *BGLAP*, and *OSX* expression at day 7. **f** Western blot results for pSMAD1/5, SMAD1/5, RUNX2, OSX, BMP2, and the internal control GAPDH. Ataluren promoted pSMAD1/5, RUNX2, OSX, and BMP2 expression compared with OM. **g** Quantification shows the same results as that of western blotting. All data shown are the mean ± SD in **e**, n=3. **P* < 0.05, ***P* < 0.01 by ANOVA.

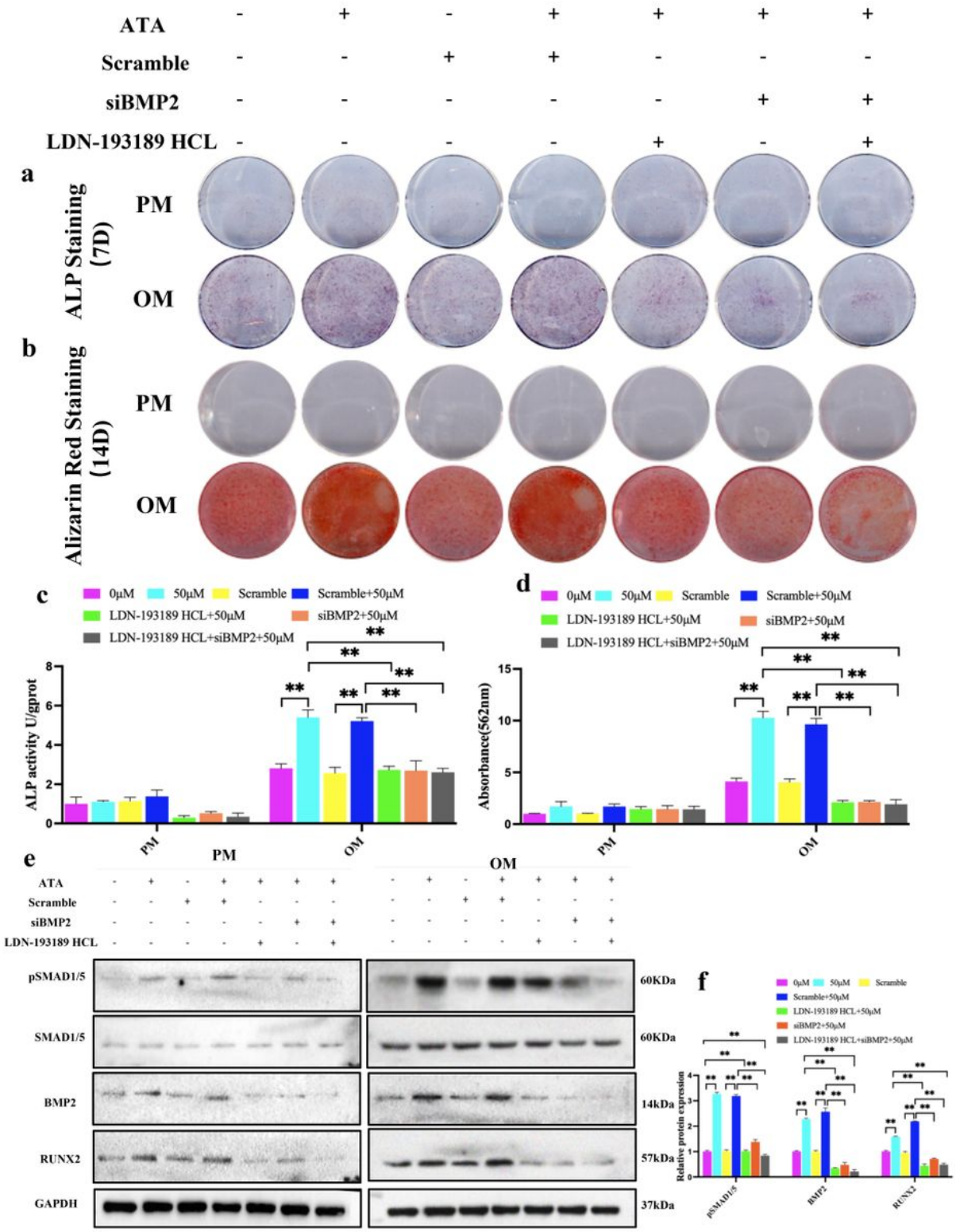


## Figure 4

The effect of ataluren on hBMMSC osteogenic differentiation relies on the BMP–SMAD pathway. hBMMSCs were incubated with PM or OM supplemented with ataluren (50 μM) together with LDN-193189 HCl or siBMP2 for 7 or 14 days. **a** In the presence of LDN-193189 HCl and siBMP2, 50 μM ataluren did not improve ALP activity in vitro. **b** In the presence of LDN-193189 HCl and siBMP2, ataluren no longer increased mineralization in hBMMSCs. **c** The ALP activity quantification results were identical to that of

ALP staining. **d** The ARS semi-quantification results agreed with that of ARS staining. The hBMMSCs were starved in FBS-free medium for 6 h before LDN-193189 HCl treatment. **e** Western blotting for the protein expression of SMAD1/5, pSMAD1/5, BMP2, RUNX2, and the internal control GAPDH at 7 days. **f** Quantification shows the same results as that of western blotting of the OM-treated group (right panel in e). All data shown are the mean ± SD in **c d f**, n=3. **P* < 0.05, ***P* < 0.01 by ANOVA.

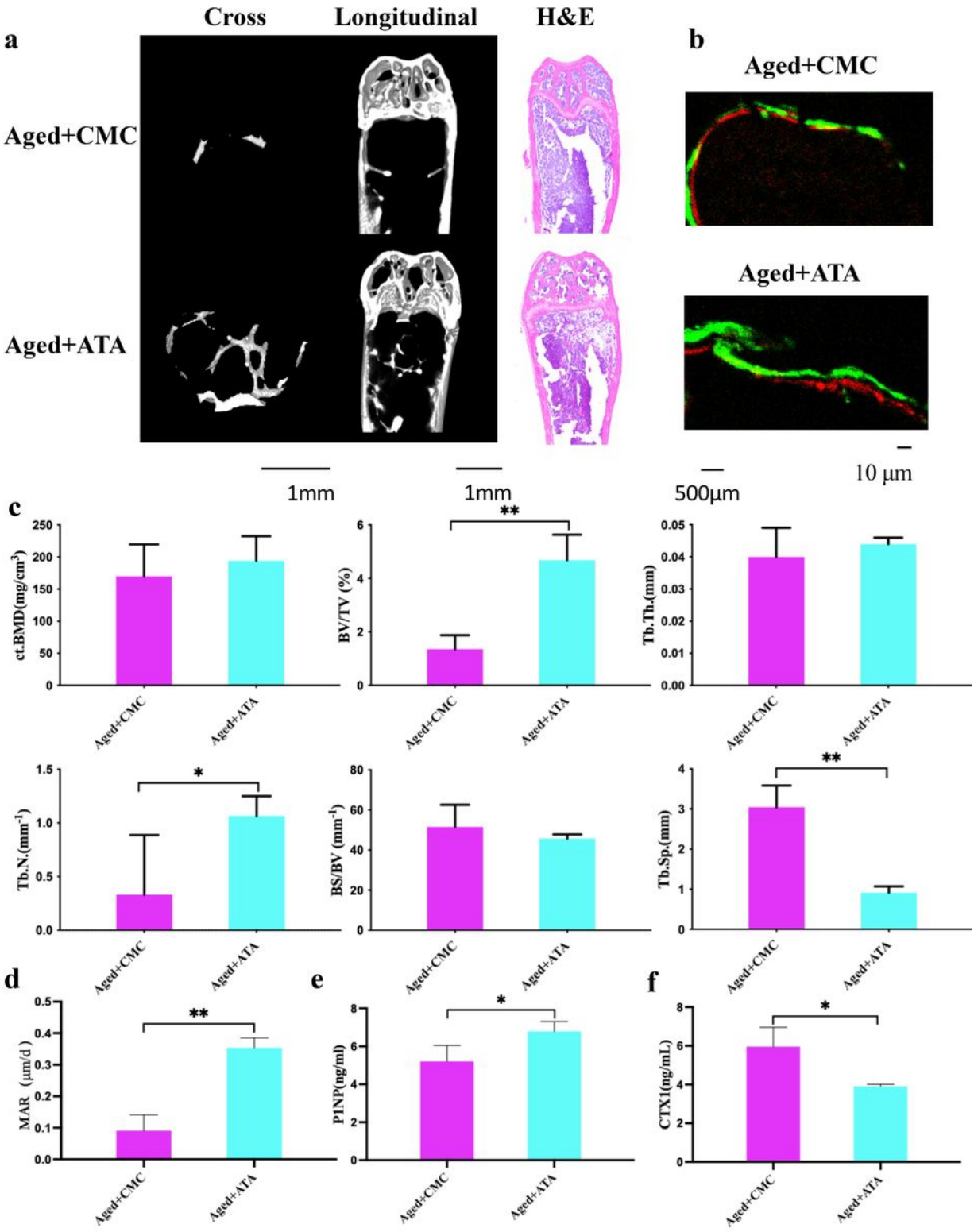


Figure 5

Ataluren partially reversed bone loss in aged mice. **a** Micro-CT (left), H&E staining (right) images of Aged+CMC and Aged+ATA mice. Micro-CT images are at a scale of 1 mm. H&E-stained images are at a scale of 500 μm. **b** Representative images of new bone formation in the distal femoral epiphysis assessed by calcein and alizarin-3-methyliminodiacetic acid double-labeling. Scale bar, 10 μm. **c** Compared to Aged+CMC mice, ataluren-treated aged mice had improved BV/TV and Tb.N and significantly reduced Tb.Sp. **d** Mineral apposition rates (MAR) of Aged+CMC and Aged+ATA mic. **e** Serum levels of PINP. **f** Serum levels of CTX-1. All data shown are the mean ± SD in **c d e f**, n=5. *$P$< 0.05, **$P$< 0.01, when comparing with Aged+CMC control group by Student's t test.

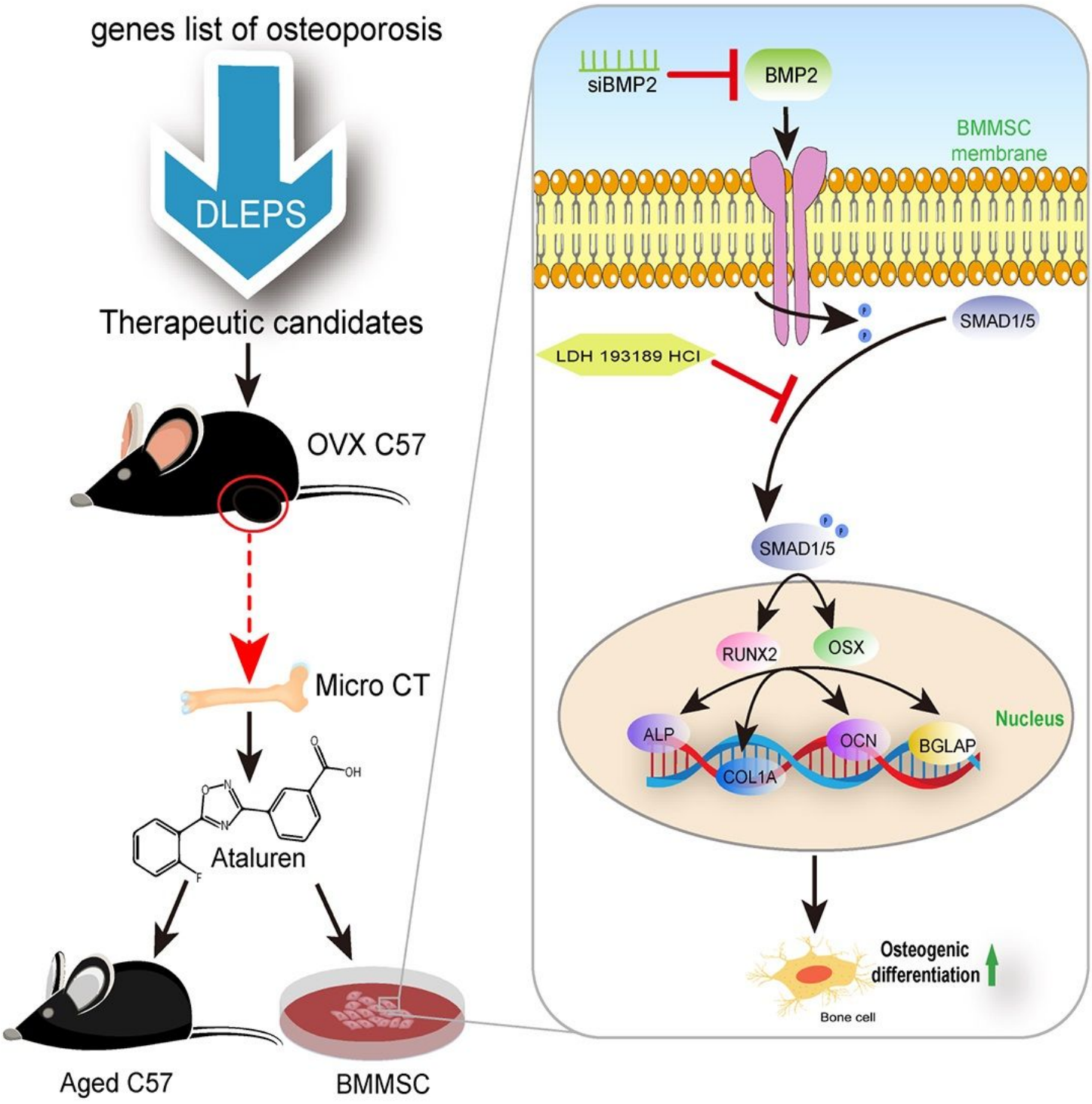


**Figure 6**

Graphical mechanism of ataluren.

## Supplementary Files

This is a list of supplementary files associated with this preprint. Click to download.

- Additionalfile1.docx
- Additionalfile2TableS2.xlsx
- Additionalfile3TableS3.xlsx
- Additionalfile4.docx
- Additionalfile5.docx
- Additionalfile6.docx